Effect of the Molecular Weight of Maleated Polypropylenes on the Melt Compounding of Polypropylene/Organoclay Nanocomposites

Yeh Wang, Feng-B. Chen, Kai-C. Wu

Department of Chemical Engineering, Tunghai University, Taichung, Taiwan, 407, Republic of China

Received 3 March 2004; accepted 4 October 2004
DOI 10.1002/app.21557
Published online in Wiley InterScience (www.interscience.wiley.com).

ABSTRACT: Maleic anhydride grafted polypropylene (PP-*g*-MA) and organically modified clay composites were prepared in a plasticorder. PP-*g*-MAs, including Polybond PB3150, Polybond PB3200, Polybond PB3000, and Epolene E43, with a wide range of maleic anhydride (MA) concentrations and molecular weights were used. The structure was investigated with X-ray diffraction (XRD) and transmission electron microscopy (TEM). PP-*g*-MA compatibilizers gave rise to similar degrees of dispersion beyond the weight ratio of 3/1, with the exception of E43, which had the highest MA content and the lowest molecular weight. The thermal instability and high melt index were responsible for the ineffective modification by E43. Furthermore, PP-*g*-MA with a lower molecular weight and a higher melt index had to be compounded at a lower mixing temperature to achieve a reasonable level of torque for clay dispersion. Polypropylene/organoclay nanocomposites were then modified with different levels of PP-*g*-MA compatibilizers with a twin-screw extruder. The polypropylene/E43/clay system, as shown by XRD patterns and TEM observations, yielded the poorest clay dispersion of the compatibilizers under investigation. The curves of the relative complex viscosity also revealed a systematic trend with the extent of exfoliation and showed promise for quantifying the hybrid structure of the nanocomposites. The mechanical properties and thermal stability were determined by dynamical mechanical analysis and thermogravimetric analysis, respectively. Although PP-*g*-MA with a lower molecular weight led to better clay dispersion in the polypropylene nanocomposites, it caused deterioration in both the mechanical and thermal properties of the hybrid systems. © 2005 Wiley Periodicals, Inc. J Appl Polym Sci 97: 1667–1680, 2005

Key words: compatibilization; melt; nanocomposites; organoclay; poly(propylene) (PP)

INTRODUCTION

Since the first mass production of isotactic polypropylene (PP) with the development of Ziegler-type catalysts, commercial exploitation has been very rapid because of PP's attractive characteristics, including low cost, low weight, a heat distortion temperature above 100°C, and extraordinary versatility in terms of properties, applications, and recycling. The consumption growth rates have been high, with the material becoming widely used in various industrial areas for fibers, films, and injection-molding articles. The further modification of PP by the addition of fillers, reinforcements, or blends of special monomers or elastomers can render it more flexible with a variety of other properties, and its competitiveness in engineering resin applications has greatly improved. The addition of nanoscopic fillers of high anisotropy in polymer matrices is, therefore, very interesting in the polymer industry.[1,2] This interest stems from the fact that when these nanoscopic fillers are used instead of conventional reinforcements, the composite materials exhibit a wide range of enhanced performance, including mechanical, thermal, and gas-barrier properties, at relatively low loadings.[3–5] The enhanced reinforcement is a result of the much greater surface-to-volume ratios of these high-aspect-ratio fillers.

Among the various kinds of natural and synthetic clays, the most common nanoscopic filler is derived from montmorillonite (MMT) clay, which is found naturally in a layered silicate structure with a high surface area (ca. 750 m^2/g). The clay exists in a tactoid structure of 20–25 layers, and this translates into an aspect ratio of about 10. Exchanging the cations between the silicate layers with the bulkier and more organophilic cations, such as a long-chain alkylammonium ion, alters the clay structure, and this is called organoclay. The cations expand the layer or basal spacing; and the increased spacing makes it possible for the clay layers to be intercalated and exfoliated. Exfoliated clay is desirable because exfoliation creates individual clay platelets, which are approximately 1

Correspondence to: Y. Wang (yehwang@mail.thu.edu.tw).
Contract grant sponsor: Union Chemical Laboratories of the Industrial Technology Research Institute.

nm thick and have an aspect ratio of approximately 100. It is very common for these systems to be made of partially exfoliated clay in a combination or hybrid structure, in which some of the clay exists in the intercalated state and the rest exists in the exfoliated state.

Although anisotropic nanofillers afford attractive combinations of stiffness and toughness, the dispersion problems due to strong particle interactions of nanofillers have limited their applications. Different routes to the formation of polymer/organoclay nanocomposites have been reviewed in the literature,[4–8] and a number of paths leading to the dispersion of nanofillers have been proposed for preparing nanocomposites. However, melt intercalation and layer separation have become the two dominant ways of preparing polymer/clay nanocomposites because of their cost effectiveness. Melt intercalation involves the mixing of clay with a molten polymer matrix. Layer separation, especially exfoliation, depends on the establishment of favorable interactions between the polymer and the clay surface and subsequent system energy reduction. Examples can be found for polystyrene,[9–12] poly(ethylene oxide),[13] and nylon.[14–16] More recently, direct melt intercalation has been recognized as a promising approach because of its ease with conventional polymer mixing or extrusion processes and its environmental benignancy.

On the basis of the melt delamination or exfoliation of organoclay, a two-stage mechanism has been proposed.[10,11,16] During the first stage, the polymer melt-intercalates into expanded clay galleries, and the polymer chains need to be transported from the bulk melt into the silicate interlayers. They then enter the clay galleries and push the ends of the platelets apart. This pathway does not require high shear but involves the diffusion of the polymer from the bulk into the clay galleries. The major driving force is either the physical or chemical affinity of the polymer for the organoclay surface, and the enthalpy of mixing can be rendered favorable by maximization of the driving force. This is relevant to polymers with polar groups compatible with the polar hydroxyl groups on silicate clay layers. During the second stage, the clay tactoids are exfoliated under shear, stacks of clay platelets are reduced in height as platelets slide apart from one another, and the contact area between the resin matrix and clay platelets is increased. A high shear intensity helps the formation of polymer/clay hybrids by breaking up clay particles and increasing sample uniformity. The process is thus facilitated by both the residence time and screw configuration in the extruder.

For nonpolar polymers such as PP, unless the surface of the organoclay is further treated with compatibilizers, applying a high shear intensity during melt processing does not cause the clay tactoids to delaminate. Efforts have been made to improve the mixing of clay in PP with functional oligomers as compatibilizers[17–23] through the grafting of a polar component such as maleic anhydride (MA) to the nonpolar polymer backbone. This produces a functionalized polymer that is compatible with the clay and also miscible with the bulk polymer matrix. Exfoliated and intercalated structures have been observed in modified PP/organoclay composites. In short, the addition of the compatibilizers creates more favorable polymer–clay interactions and leads to the exfoliation of the clay layers.

The chemical properties of maleated PP that influence its effectiveness as a compatibilizer for PP/organoclay nanocomposites are (1) the molecular weight, which determines the magnitude of the shear viscosity and melt index (MI), and (2) the MA content, which is related to the amount of functionality present in the compatibilizer. Several studies concerning the effects of compatibilizers on the clay dispersion via the melt process have been reported.[18–20,22,24,25] The effect of the MA content on the clay dispersion has been studied extensively, but the results are somewhat inconsistent. A high MA concentration generally enhances the melt intercalation of PP oligomers into clay layers; however, it may lead to immiscibility with the PP matrix[18] and harm the mechanical properties of the composites. However, some authors have still found that a high MA concentration (4.2%) improves the mechanical strength better than a low MA concentration (2.9%) with the same composition.[22] Because the mechanical properties are also affected by the compatibilizer loading, we need to be careful when assessing the results from different sources.

However, the effect of the molecular weight is less clear. Most authors have used low-molecular-weight PP oligomers to enhance the diffusion of oligomers into clay galleries.[18–20,22] However, Wang et al.[24] found that although a low-molecular-weight [weight-average molecular weight (M_w) = 9100] oligomer resulted in better dispersion, a high-molecular-weight (M_w = 330,000) compatibilizer better improved the mechanical properties. In a study by Kim et al.,[25] four PP compatibilizers with various degrees of MA grafting and three PP matrices of low, medium, and high viscosities were used. Low-viscosity PP with the compatibilizer of the lowest MA concentration (0.55%) resulted in the greatest improvement of the dynamic storage modulus (E'). Without the molecular weight of the compatibilizer, it is hard to judge the importance of the viscosities of individual components. Regardless of the type of maleic anhydride grafted polypropylene (PP-*g*-MA), the weight ratio of PP-*g*-MA to organoclay was roughly 3 so that the maximum improvement in the mechanical properties could be achieved. As expected, too high a fraction of PP-*g*-MA is detrimental to mechanical properties because the physical properties of compatibilizers are

usually inferior to those of the polymer matrix, and too low a fraction of PP-*g*-MA makes it impossible to reach a desirable degree of clay dispersion. There is an optimum composition for individual maleated PP to be incorporated into PP/organoclay nanocomposites.

In this study, PP has been melt-mixed with organic MMT and various kinds of PP-*g*-MA with a broad range of MA contents and molecular weights. However, an admixture of the polymer and organoclay may be transformed into an exfoliated or intercalated nanocomposite or a conventional macrocomposite. The process depends critically on the characteristics of the ingredients, such as the rheological and thermodynamic nature of the matrix polymer and compatibilizer and the type, packing density, and size of the organic modifier on the silicate surface. Although the underlying principles of intercalation are well documented, most studies have been conducted for direct melt compounding under intuitive processing conditions within a limited range of MA contents, and the effect of the molecular weight of maleated PP has been rarely discussed. In addition, it might be thought that the melt-processing conditions have a significant impact on the nature of the nanocomposites formed. Unfortunately, until recently, the literature has contained no firm conclusions on the processing conditions. This study provides fundamental information required for the successful production and application development of PP-based composites and sheds some light on the interactions between the chemistry of compatibilizing organoclay and the processing conditions.

EXPERIMENTAL

Materials

Injection-grade isotactic PP homopolymer (Yungsox 1040), provided by Yung-Chia Chemical Co. (Taiwan), was used as the base polymer in this study. The density of PP was 904 kg/m^3, as measured with an electronic densimeter. Octadecylamine-modified MMT clay (Nanomer I.30 P) via cation exchange was used as the organoclay. The initial basal spacing was 2.36 nm, and it was used as received from Nanocor. The four types of compatibilizers—Polybond PB3150, Polybond PB3200, Polybond PB3000, and Epolene E43—were MA-modified PPs with MA concentrations of 0.5–4.0 wt %. The physical properties of the base polymer and the compatibilizers are summarized in Table I. To all the compounds, a 0.2 wt % heat stabilizer (Evernox-10) from Everspring Chemical Co. (Taiwan) was added to prevent the degradation of the polymer during the compounding. PP and the stabilizer were dry-blended at room temperature after dehumidification.

TABLE I
Physical Properties of the PP Matrix and Compatibilizers

Trade name	MI (g/10 min)[a]	M_w (g/mol)	T_m (°C)[b]	MA content (wt %)	T_d (°C)[c]
PP1040	2	—	165	—	345
PB3150	20	330,000[d]	164	0.5[d]	335
PB3200	115	120,000[d]	163	1.0[d]	313
PB3000	425	61,000	161	1.2[d]	293
E43	1654 (180°C)	9,100[d]	153	4.0[d]	161

[a] Determined by ASTM D 1238 at 2.16kg and 190°C.
[b] T_m = melting point determined from the peak value of the DSC scan.
[c] T_d = onset degradation temperature determined from TGA analysis.
[d] Manufacturer's data.

Compounding procedures

To determine the proper composition of the compatibilizers for the nanocomposites and critically compare the performances of the various compatibilizers, we first employed an internal mixer, a Brabender PL 2000 plasticorder (Duisburg, Germany), the for melt compounding of the composites of clay and PP-*g*-MA compatibilizers. A W 50 mixing head with a mixing volume of 60 cm^3 was installed. Before the melt processing, all the components were dried at 80°C for 24 h. The organoclay, a powder with a mean particle size of approximately 1 μm, and the powdered PP-*g*-MA were premixed in a tumbler.

The mixing temperature was set at about the melting point of the compatibilizers, the rotation speed was 100 rpm, and the total mixing time was 15 min, during which the imposed torque and temperature reached an equilibrium value.

We then prepared the PP/PP-*g*-MA/clay composites on an intermeshing, corotating, self-wiping, twin-screw extruder in the corotating mode. The PSM30 machine was manufactured by Sino-Alloy Machinery, Inc. (Taiwan), and had a screw diameter of 31.2 mm, a distance between screw axes of 26.2 mm, a screw-tip clearance of 0.25 mm, and a length/diameter ratio of 45. The screw consisted of 10 segmented barrels with three kneading zones. The first kneading zone started at the second barrel, consisting of high-shear disk blocks, and ended with neutral blocks. The second one started at the fourth barrel and also consisted of high-shear elements with reverse elements at the end. The third one started at the seventh barrel with a wide-pitched low-shear element. In the first and second kneading zones, more severe shearing action was assumed because of the high-shear disk blocks and the presence of reverse-flight elements. The reverse elements increased the resistance to flow and resulted in an increase in the fill degree and the residence time in the mixing section. The wide-pitched element only

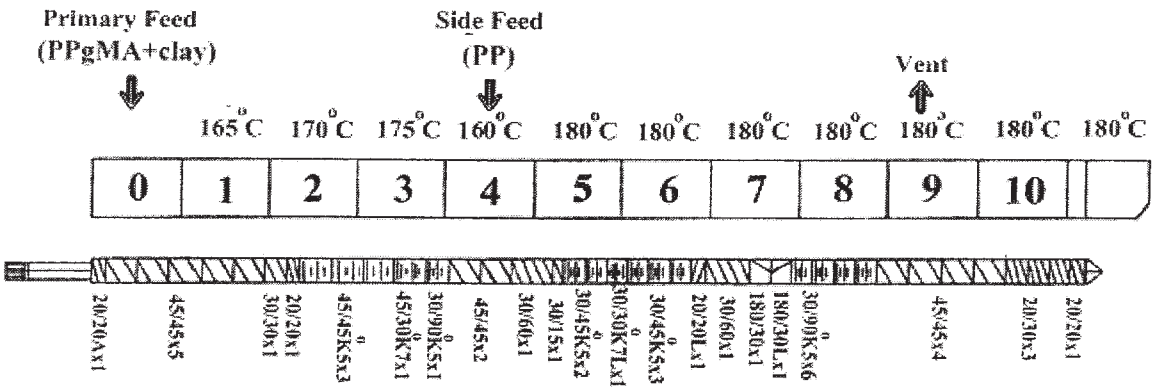

Figure 1 Schematic of the twin-screw configuration and barrel-temperature profiles of the PSM30 machine.

induced gentle shearing and homogenization of the polymer melt.[15,16] Therefore, the filler particles were expected to experience a high intensity of dispersive mixing in the first and second kneading zones, and the distributive mixing action dominated in the third kneading zone. The details of the screw configuration and element geometries are shown in Figure 1. A standard pelletizing die plate was installed at the screw end. The strand was solidified in a water bath and pelletized.

In addition to the screw configuration, the principal processing variables were the throughput rate, screw speed, and barrel-temperature profiles. After several trials, the screw speed was set at 200 rpm, and the barrel temperatures were set from 165°C at the first barrel to 180°C at the last barrel. The barrel-temperature profiles are also shown in Figure 1. The screw speed and the barrel temperatures were fixed for all the experimental runs. Moreover, the throughput rate was fixed at about 3.5 kg/h.

Furthermore, the polymer pellets, powdered PP-*g*-MA, and clay were metered independently in the required proportions with volumetric dosing units. To achieve a desirable modification of the clay, the premixed organoclay and PP-*g*-MA were fed into a secondary feeding port with a forced feeder, and the PP pellets were introduced separately through the main hopper.

Structural characterization

Structural characterization (degree of delamination and dispersion) was carried out with transmission electron microscopy (TEM) and X-ray diffraction (XRD). The TEM instrument used in this study was a JEOL JEM-1200EX II (Tokyo, Japan) with a 120-kV electron accelerator. Sixty-to-ninety-nanometer sections were prepared from the pellets via melt compounding on a twin-screw extruder. The sections, mounted on a 200-mesh copper grid, were cut with a microtome procedure with a diamond knife; the sample was held at room temperature to produce the uniform thin sections required to obtain clear, reproducible images. The TEM results (3-in. × 5-in. prints with a print magnification of 10,000–60,000×) were categorized by the averaging of the number of platelets or intercalates in 12-in.^{2} cutouts.

The characterization of the structure by XRD was carried out for powdered samples from the pellets. The XRD instrument was a MacScience M18XHF-SRA X-ray diffractometer (MacScience Co., Ltd. Yokohama, Japan). The diffractometer was equipped with a Cu Kα radiation source and was operated at 40 kV and 100 mA. The data were recorded in the reflection mode over a 2θ range of 2–10° at a rate of 2°/min; the measurements were taken at equal increments of 0.02°.

Rheological characterization

The granules were compression-molded with a hydraulic press with 7 kg/cm^2 (100 psi) of pressure at 180°C for 20 min. The compressed disks were 25 mm in diameter and 0.9 mm thick. The rheological characterization was carried out on a Rheometrics RDAII (Piscataway, NJ). A frequency range of 0.1–100 rad/s and a strain of 6% were applied during the measurements. A strain sweep was performed to verify that the strain amplitude was within the linear viscoelastic regime.

Mechanical characterization

Dynamic mechanical analysis (DMA; model 7e, PerkinElmer, Wellesley, MA)) was used to assess the mechanical performance of the composites. The dynamic moduli of the hybrids versus the temperature were obtained by the sinusoidal vibration of the samples in the three-point-bending mode at 1 Hz. The vibration amplitude was 5 μm. The temperature range was −30–170°C, and the heating speed was 2°C/min.

TABLE II
Experimental Conditions for the Plasticorder (100 rpm, 15 min)

No.	Composition (PP-*g*-MA/clay)	Mixing temperature (°C)	Equilibrium temperature (°C)	Equilibrium torque (Nm)
1	PB3150/I30 = 1	160	186	13
2	PB3150/I30 = 2	160	180	10.2
3	PB3150/I30 = 3	160	178	9.3
4	PB3150/I30 = 4	160	177	8.6
5	PB3150/I30 = 6	160	176	7.9
6	PB3150/I30 = 8	160	175	7.1
7	PB3150/I30 = 10	160	174	6.5
8	PB3200/I30 = 3	155	173	9.7
9	PB3200/I30 = 4	155	169	7.1
10	PB3200/I30 = 8	155	165	4.8
11	PB3200/I30 = 10	155	164	4.1
12	PB3000/I30 = 3	150	167	8.7
13	PB3000/I30 = 4	150	164	7.3
14	PB3000/I30 = 8	150	161	5.7
15	PB3000/I30 = 10	150	158	4.9
23	E43/I30 = 1	140	152	7.1
24	E43/I30 = 2	140	146	3.5
25	E43/I30 = 3	140	145	2.3
26	E43/I30 = 4	140	144	1.4
27	E43/I30 = 6	140	144	0.8
28	E43/I30 = 8	140	144	0.3
29	E43/I30 = 10	140	144	0.1

Thermogravimetric analysis (TGA)

TGA (TGA 951, TA, New Castle, DE) was used to evaluate the thermal stability of the PP nanocomposites. The chamber was flushed with nitrogen. The temperature range was 30–500°C, and the heating speed was 10°C/min.

RESULTS AND DISCUSSION

We first investigated composites of clay and PP-*g*-MA compatibilizers prepared in the plasticorder in hope of finding guidelines for the suitable loading of compatibilizers in PP/clay composites prepared on a twin-screw extruder. Therefore, the exfoliation or intercalation behavior of PP-*g*-MA/clay composites was examined at various loadings for the four types of compatibilizers. MA-functionalized compatibilizers have been used for preparing nanocomposites in olefinic polymers such as PP and polyethylene.[6] According to a literature review, the exfoliation of layered silicates is generally enhanced by the loading of PP-*g*-MA being increased. However, there are many differences in the characteristics of the compatibilizers reported in the literature. Thus, various molecular weights and MA contents in PP-*g*-MA and various processing parameters such as the operating temperature and mixing time have been employed. Nevertheless, the molecular weight of the compatibilizer and the shear intensity for complete exfoliation have not been clarified. In addition, the relationship between the compatibilizer chemistry and the processing conditions should be coupled because both might affect the exfoliation behavior. Thus, these two factors should be considered at the same time.

Clay dispersion in pp-*g*-MA/organoclay nanocomposites

Detailed experimental conditions for the plasticorder are listed in Table II for clay blended with PB3150, PB200, PB3000, and E43. The weight ratio of PP-*g*-MA to clay was varied from 1 to 10 for investigating the degree of clay exfoliation under fixed operating conditions; the rotation speed was 100 rpm, and the mixing time was 15 min. The mixing temperature was determined according to the melting point of each compatibilizer. Hence, the compatibilizer with a high molecular weight and a low MI was compounded at a higher temperature than that with a low molecular weight and a high MI.

In addition, the equilibrium torque and the equilibrium temperature were included. For effective compounding in the plasticorder, the equilibrium torque had to be maintained at a certain level; therefore, the equilibrium temperature for the compatibilizer with a high MI had to be lower than that for the compatibilizer with a low MI. Furthermore, as the ratio of PP-*g*-MA to the clay increased, the torque decreased because the shear viscosity of the composite decreased with an increasing weight fraction of PP-*g*-MA. At the same weight fraction, the E43/clay composites showed the lowest torque of all the composite sys-

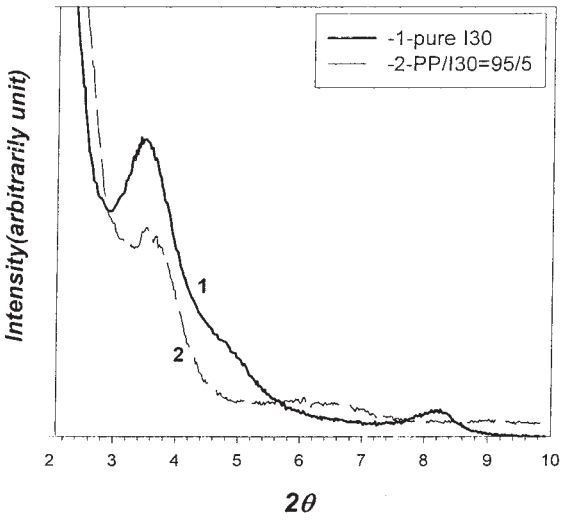

Figure 2 XRD patterns of pure I30 and unmodified PP/I30 composites.

tems. Particularly at high weight fractions of E43, the equilibrium torque dropped to nearly zero. Such a low level of torque led to poor compounding of the E43/clay composites, as we discuss later.

We then examined the structure of the composites. Figure 2 shows the XRD patterns of the PP/I30 composite and pure I30. The (001) plane peak of the PP/I30 composite containing 5 wt % I30 was observed at $2\theta = 3.75°$ (2.35 nm), whereas the peak of the pure clay I30 was observed at $2\theta = 3.74°$ (2.36 nm). This indicated little change in the basal spacing of clay I30 in the PP/I30 composite, and this was due to the incompatibility of the polar hydroxyl groups on the surface of the clay layers and the nonpolar PP.[18,22,24] Next, we show the X-ray powder diffraction patterns for composites of I30 and compatibilizers. The results are displayed in Figure 3(a,b) for PB3150/I30 and E43/I30 systems, respectively. As indicated in these XRD diffractograms, the clay characteristic peak height decreased with an increasing loading of the compatibilizers. Although a distinct shift to a lower angle could be observed [Fig. 3(a)] as the weight fraction of PB3150 increased, the peak shifted to higher angles in the E43/clay systems as the weight fraction of E43 increased [Fig. 3(b)]. As mentioned previously, low torque during compounding led to the poor dispersion of clay layers in the E43 matrix, even though E43 had a high MA content. Furthermore, no more diffraction peaks were visible over the weight ratio of 4 in the PB3150/I30 composites. No diffraction peak for clay has generally been accepted as meaning that no ordered structure in a specimen exists, and it is necessary for complete exfoliation.[6] There was clearly a clay characteristic peak at the weight ratio of 3 for the PB3150/I30 composite, although it was small. It was difficult to determine the peak location because of the peak's broadness. However, the clay characteristic peaks were only found up to 3 for PB3150/clay composites. Therefore, we concluded that the ordered structure of the clay layers disappeared in the weight ratio range of 3–4 under the operating conditions of 100 rpm and a 15-min mixing time.

Figure 4(a,b) shows the XRD patterns of the compatibilizer/I30 composites with weight ratios of 3 and 10, respectively. The (001) plane peak of clay I30 shifted to lower angles in the composites with a weight ratio of 3 and nearly disappeared in the composites with a weight ratio of 10 for all kinds of PP-*g*-

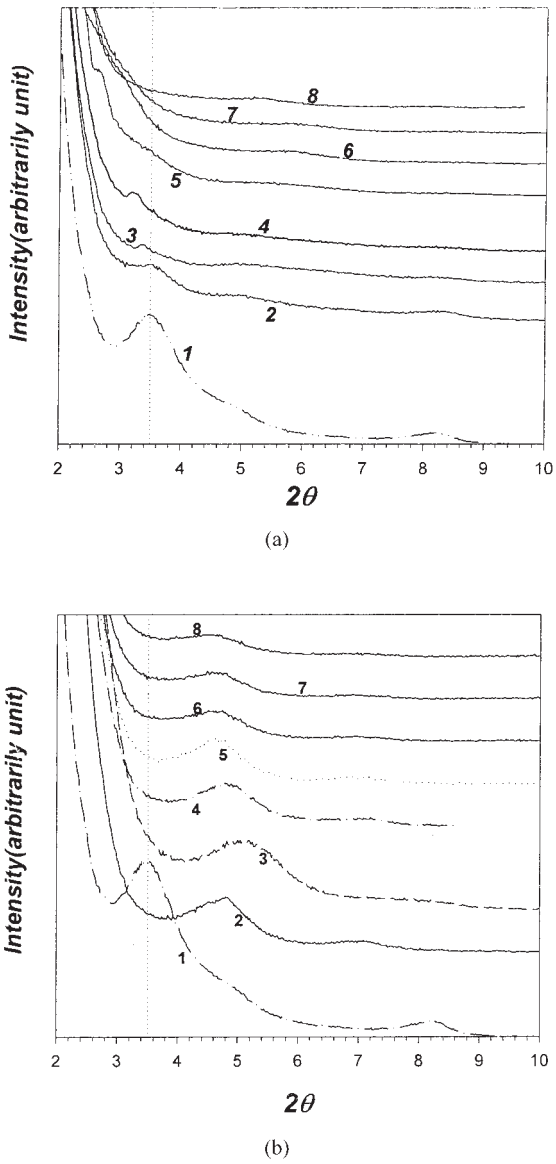

Figure 3 (a) XRD patterns of PB3150/I30 nanocomposites: (1) pure I30, (2) 1/1 PB3150/I30, (3) 2/1 PB3150/I30, (4) 3/1 PB3150/I30, (5) 4/1 PB3150/I30, (6) 6/1 PB3150/I30, (7) 8/1 PB3150/I30, and (8) 10/1 PB3150/I30. (b) XRD patterns of E43/I30 nanocomposites: (1) pure I30, (2) 1/1 E43/I30, (3) 2/1 E43/I30, (4) 3/1 E43/I30, (5) 4/1 E43/I30, (6) 6/1 E43/I30, (7) 8/1 E43/I30, and (8) 10/1 E43/I30.

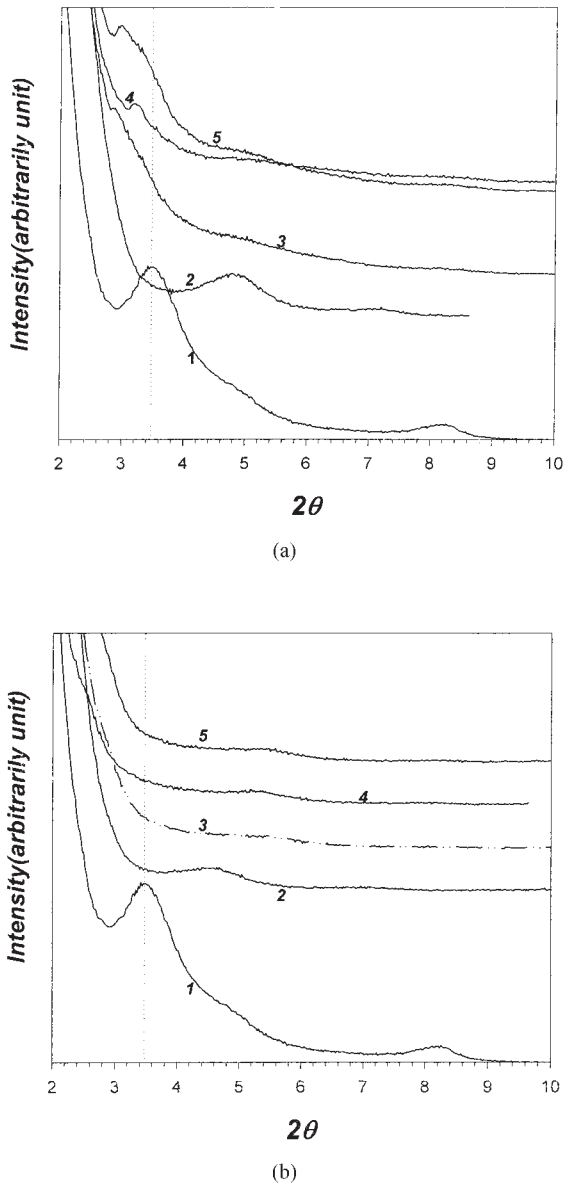

Figure 4 XRD patterns of (a) 3/1 and (b) 10/1 compatibilizer/I30 nanocomposites: (1) pure I30, (2) E43, (3) PB3000, (4) PB3150, and (5) PB3200.

MA, except for E43. As shown in Figure 4(a), the peak shifting clearly indicated an intercalation structure in these composites. It also showed different peak shifting according to the molecular weight and MA content of the PP-*g*-MA compatibilizers. If we disregard E43, the biggest peak shift occurred for the PB3000/I30 composite, PB3000 having a lower M_w value and a higher MA content than PB3150 and PB3200. Even though E43 had the lowest M_w value and the highest MA content of all the compatibilizers, the low MI of E43 led to a low equilibrium torque (see Table II) and caused the poor dispersion of clay in the E43/I30 composites. In kinetic terms, the high polarity and mobility of E43 enhanced the polymer–clay affinity and polymer chain diffusion into the clay galleries. However, it could not compensate for the low equilibrium torque, which inhibited the breakup of clay layers during compounding and limited the intercalation of E43 into clay galleries within a short mixing period of 15 min. The low initial decomposition temperature of E43 (see Table I) may also have been responsible for the poor clay dispersion. In fact, the yellowing of the E43/I30 composites was clearly observed after the compounding.

Although the disappearance of the diffraction peak under XRD scans is clearly shown in Figure 4(b), XRD scanning could not provide definitive information on the structure of the nanocomposite when the periodic arrangement disappeared in the exfoliated clay layers. It also suffered from weak peak intensity, particularly in those composites for which the clay content was small.[26] Therefore, TEM was used to supplement the XRD technique through the direct observation of the state of the dispersion of the clay platelets in the composites.

Figure 5(a,d) presents TEM micrographs for PP-*g*-MA/I30 nanocomposites with the weight ratio of 10. At the magnification of 60,000×, both thick and dark strips and thin and gray lines can be seen clearly. The dark strips, which may represent stacks of silicate layers, indicate the breakup of the clay tactoids. The existence of characteristic peaks in the XRD patterns should be attributed to the intercalated silicate layers in the stacks. On the other hand, the gray lines, which may represent single layers or small stacks of clay platelets, indicate a state of complete exfoliation in the matrix. The thin and gray lines thus represent clay nanolayers within the resolution provided. Either the clay stacks (shown as dark strips) or nanolayers (shown as gray lines) were well dispersed. However, in Figure 5(d) for the E43/I30 system, only large clay aggregates with a few dark strips can be seen. The E43 compatibilizer apparently did not even intercalate into the clay galleries. The TEM observations support the XRD diffraction patterns shown in Figure 4(b), in which the characteristic peaks are shifted to higher angles. Figure 6(a–c) presents TEM micrographs at a lower magnification of 10,000× for the Polybond series. Some clay particles were still poorly dispersed as microaggregates in the continuous polymer phase. Furthermore, in Figure 6(d), which shows the morphology of the E43/I30 system, the clay particles can be seen as large agglomerates that are several hundreds of nanometers or bigger. Figure 7 shows the particle size distributions derived from the TEM images in Figure 6. The long tail of the E43/I30 composites indicated the poor dispersion of clay, and the largest fraction of nanosize particles in the PB3000/I30 composites clearly revealed the effective exfoliation of clay layers by PB3000. However, the particle size distributions of the Polybond compatibilizers were not

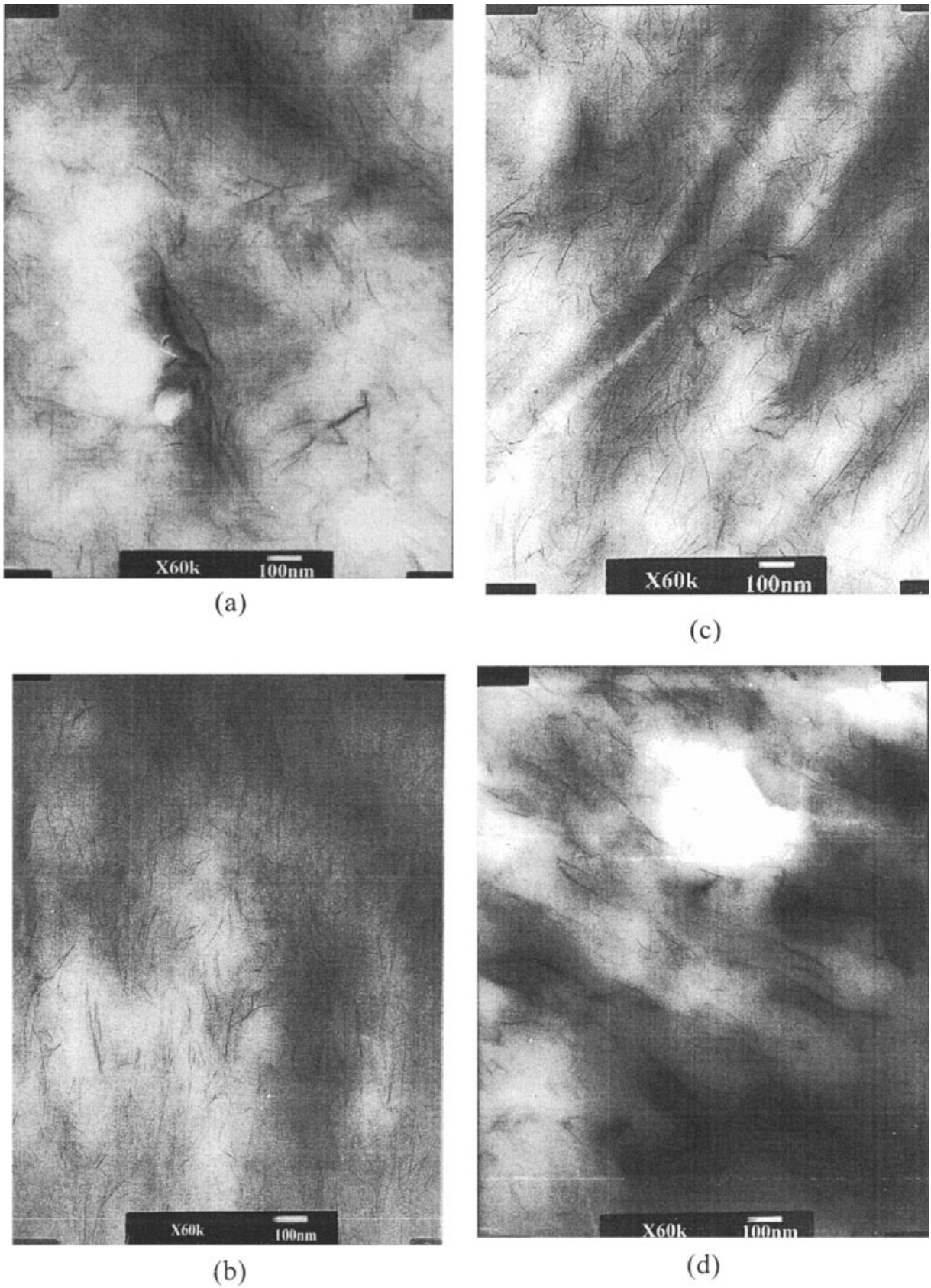

Figure 5 TEM micrographs (original magnification = 60,000×) of (a) 10/1 PB3150/I30, (b) 10/1 PB3200/I30, (c) 10/1 PB3000/I30, and (d) 10/1 E43/I30 nanocomposites.

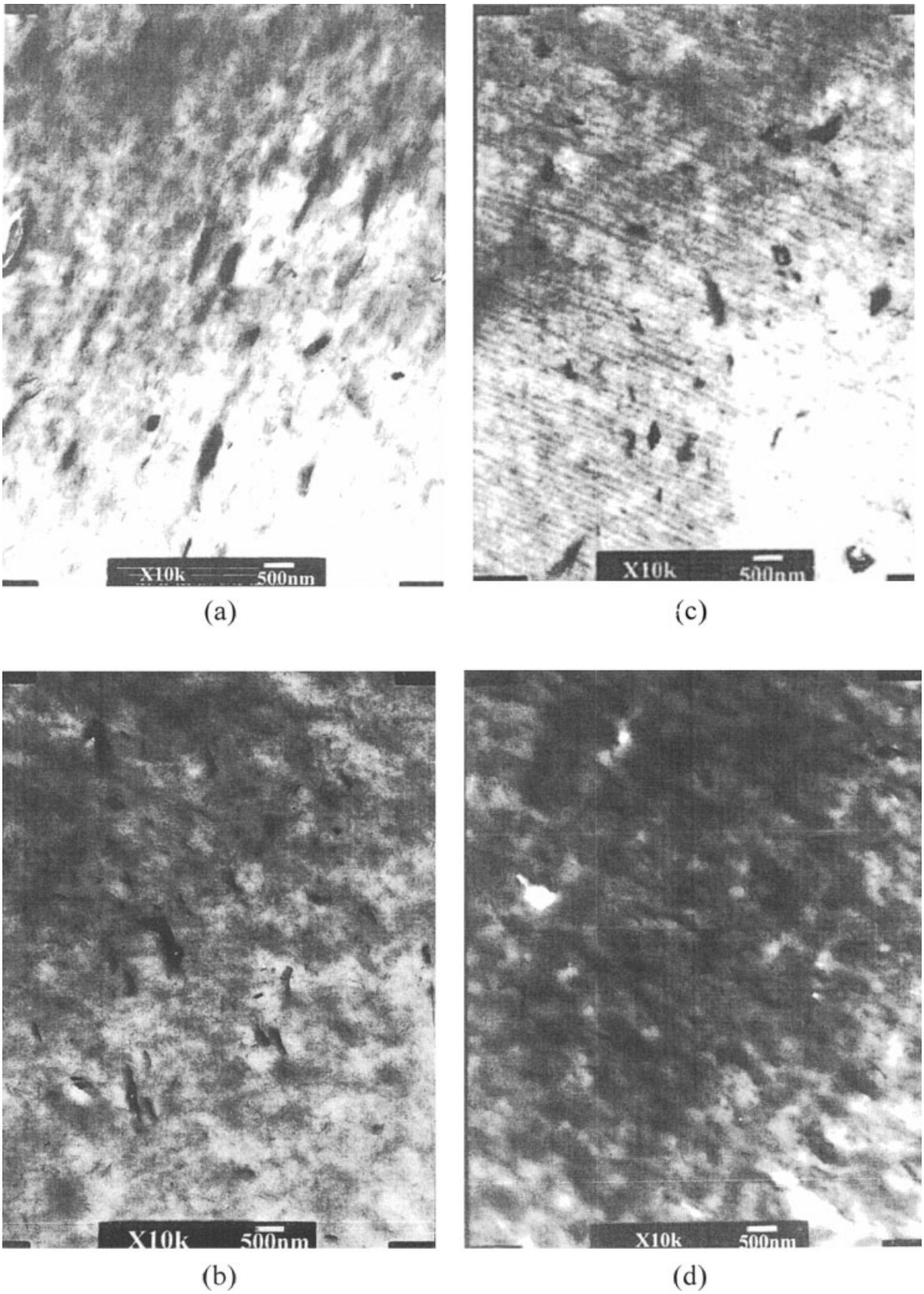

Figure 6 TEM micrographs (original magnification = 10,000×) of (a) 10/1 PB3150/I30, (b) 10/1 PB3200/I30, (c) 10/1 PB3000/I30, and (d) 10/1 E43/I30 nanocomposites.

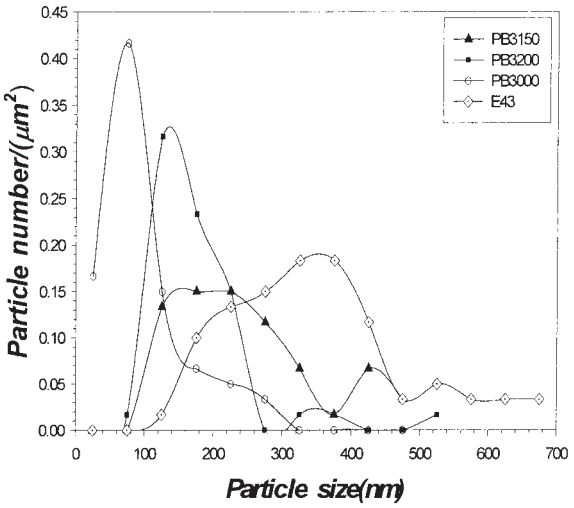

Figure 7 Particle size distribution from the TEM images in Figure 6.

significantly different. Indeed, except for the E43 systems, the modified nanocomposites exhibited a state of partial exfoliation.

Effect of PP-*g*-MA on the clay dispersion in PP/organoclay nanocomposites

The previous discussion shows that the intercalation power of the compatibilizers could be realized at a weight ratio of roughly 3, regardless of the differences in the compatibilizers. Therefore, we used weight ratios around that value in the following formulations for modifying PP/I30 composites. Direct evidence of the intercalation was provided by the XRD patterns of the obtained hybrids. Figure 8 shows the XRD patterns of PP/I30 nanocomposites modified with the four grades of compatibilizers at a weight ratio of 80/15/5 from the twin-screw extruder. It does not show any significant difference from the patterns of the compatibilizer/I30 composites; that is, the characteristic peak of I30 shifted to lower angles for all the samples except the E43/I30 composites. This clearly indicates the intercalation of the polymer chains between the silicate layers. In addition, the XRD patterns exhibit relatively small and unapparent peaks or shoulders with a gradual increase in the diffraction strength toward low angles. Completely dispersed composites exhibit no peak but a gradual increase in the diffraction strength.[6,18] Therefore, the clay layers in the composites may have been exfoliated and dispersed.

To further assess the exfoliated structure, the dispersion of the silicate layers was also observed with TEM. Figure 9(a–d) shows TEM micrographs at a high magnification of 60,000× of compatibilizer-modified PP/I30 composites. In Figure 9(a–c), for nanocomposites modified by compatibilizers of the Polybond series, the gray lines are the intersections of silicate layers 1 nm thick. Each layer of the clay was dispersed homogeneously in the PP matrix, although a small number of intercalated layers (but unexfoliated) still existed. The existence of small peaks in the XRD patterns could be attributed to these intercalated layers. On the other hand, the dark areas indicate that the clay platelets were poorly dispersed as aggregates in the continuous PP phase in the E43-modified system [see Fig. 9(d)]. During the evolution of the phase structure after the incorporation of the compatibilizer, an extra contribution arose from the specific interaction derived from hydrogen bonding between the silicate layer and MA group. This interaction was undoubtedly beneficial for overcoming the energy barrier to form randomized delamination of silicate layers, that is, an exfoliated structure. However, it was possible to induce immiscibility with the PP matrix because of an excessive MA concentration.[18] Fortunately, within the range of MA concentrations employed in this study, we did not observe any problem of immiscibility between the compatibilizer and PP matrix.

Besides the local techniques of XRD and TEM, rheological characterization is another sensitive method for revealing the global state of dispersion in composites.[27,28] The melt viscosity of these hybrid polymer nanocomposites was related to the aspect ratio of the individual fillers. The aspect ratio of the filler was then related to the intercalation of the clay. Therefore, the aspect ratio changed according to the different levels of intercalation and exfoliation. Figure 10(a) presents the complex viscosities of the nanocomposites (80/15/5) and neat PP.

On the one hand, the PP/PB3150/I30 composite showed the greatest enhancement in the complex vis-

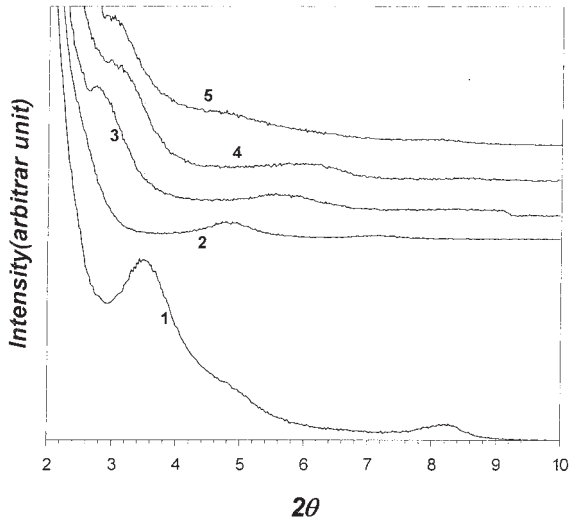

Figure 8 XRD patterns for PP-*g*-MA-modified PP/I30 nanocomposites: (1) pure I30, (2) 80/15/5 PP/E43/I30, (3) 80/15/5 PP/PB3000/I30, (4) 80/15/5 PP/PB3150/I30, and (5) 80/15/5 PP/PB3200/I30.

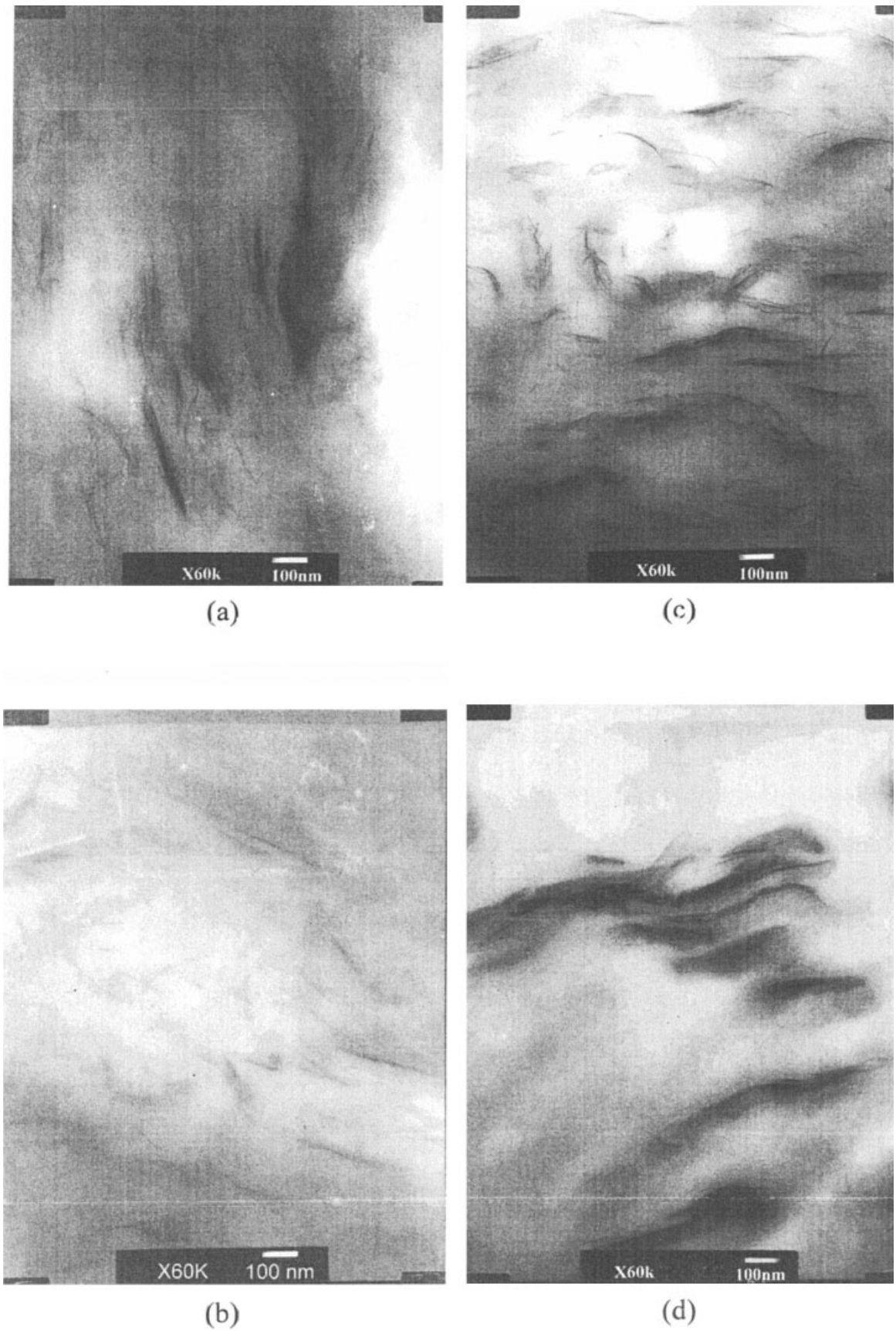

Figure 9 TEM micrographs (original magnification = 60,000×) of PP-*g*-MA-modified PP/I30 nanocomposites: (a) 80/15/5 PP/PB3150/I30, (b) 80/15/5 PP/PB3200/I30, (c) 80/15/5 PP/PB3000/I30, and (d) 80/15/5 PP/E43/I30.

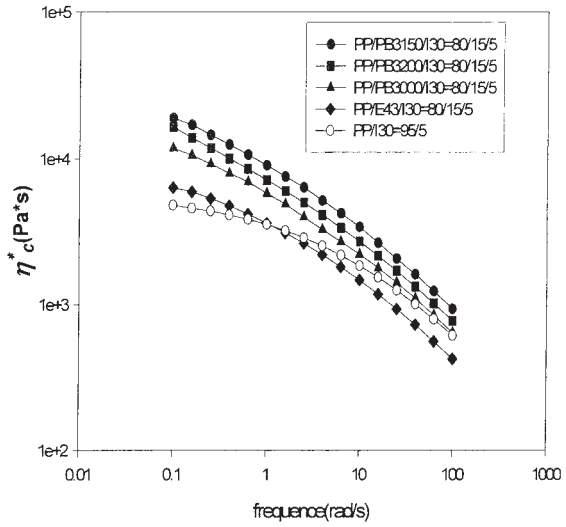

(a)

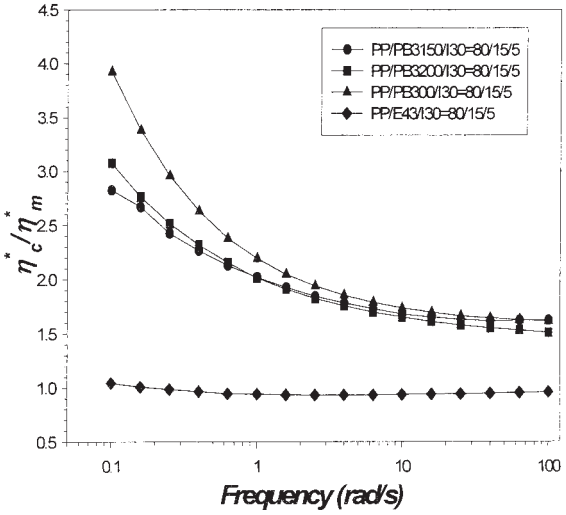

(b)

Figure 10 (a) Complex viscosity of PP-*g*-MA-modified PP/I30 nanocomposites and (b) complex viscosity of PP-*g*-MA-modified nanocomposites relative to the silicate-free PP/PP-*g*-MA matrix. η_c^* represents the complex viscosity of the nanocomposites, and η_m^* represents the complex viscosity of the corresponding matrix, which is the blend of PP and PPg MA.

cosity, mainly because of the high molecular weight of PB3150 (with the lowest MI). On the other hand, the complex viscosity of the PP/E43/I30 composite was even lower than that of neat PP. In addition to the low molecular weight of E43 (which had the highest MI), the poor dispersion of clay platelets in the composite may also have contributed to the low level of the complex viscosity. Furthermore, the enhancement of the complex viscosity was most significant in the low-frequency region for the nanocomposites modified by Polybond compatibilizers, and this may suggest a change from liquid behavior to solid behavior at low frequencies.[29] Figure 10(b) presents the relative viscosity curves of the nanocomposites modified with the different compatibilizers, relative to the silicate-free PP/compatibilizer matrix so that the effect of the filler could be isolated from that of the matrix. As expected, the PP/E43/I30 composite exhibited the least enhancement in the relative viscosity. However, contrary to the results shown in Figure 10(a), the PP/PB3000/I30 nanocomposite showed greater enhancement than the PB3150 and PB3200 systems. Under the same processing conditions, experiencing similar shear intensity because of the PP matrix, the low-molecular-weight compatibilizer may have diffused more readily into the clay galleries than the high-molecular-weight ones and resulted in a more homogeneous dispersion of clay platelets in the PP/PB3200 and 3000/I30 systems. With reference to the XRD patterns and TEM micrographs, such a procedure may be used to arrive at a representation of the global nanostructure from the relative viscosity curve for a hybrid structure. We shall pursue this subject further in a future study.

The E' values of the modified PP/I30 composites are plotted versus the temperature in Figure 11. The compositions of the modified nanocomposites were again 80/15/5All the modified PP/I30 systems exhibited similar trends in the modulus–temperature curves. There was no noticeable shift in the glass transitions in the modified systems, but the moduli of the PP/PB3150/I30 system showed the greatest improvement of all the composite systems. The E' values of the modified PP/I30 composites, relative to neat PP are plotted in Figure 12. E' of the modified PP/I30 composites clearly depended on the type of compatibilizer. In particular, the PP/PB3150/I30 system exhibited a modulus nearly 1.6 times higher than that of

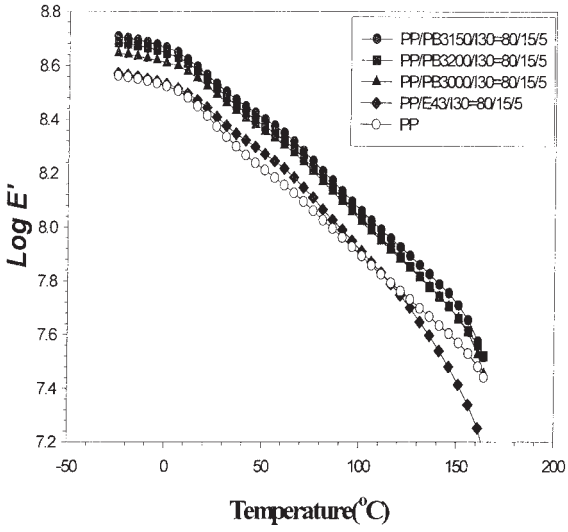

Figure 11 DMA scans of neat PP and PP-*g*-MA-modified PP/I30 nanocomposites (80/15/5).

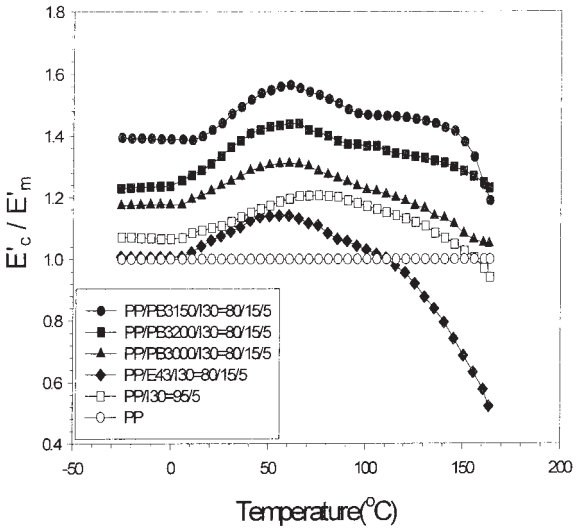

Figure 12 *E′* of PP-*g*-MA-modified PP/I30 nanocomposites relative to neat PP. E_c represents the storage modulus of the nanocomposites, and E_m represents the storage modulus of the neat PP.

neat PP at 70°C with only 5% clay. This was most likely due to the fact that PB3150 had the highest molecular weight of all the compatibilizers, with improved dispersibility of the clay layers through the addition of the compatibilizers. In addition to the clay dispersion, both the compatibilizer stiffness and loading were essential factors for achieving the maximum improvement in the composite properties.[20,24] Apparently, the relative moduli of the clay composites were higher than unity over the whole temperature range, and these were considered to be the real reinforcement effects of the clay. As expected, the PP/E43/I30 composites, which behaved like the unmodified PP/I30 composites, exhibited the least enhancement.

The thermal decomposition behavior of the neat PP and compatibilizer-modified PP/I30 composites is shown in Figure 13. The onset degradation temperatures of the nanocomposites varied from 205°C (the lowest) for the E43-modified nanocomposite to 374°C (the highest) for the PB3150-modified system. The onset degradation temperature of unmodified PP/I30 composites was 347°C, which was even higher than that of the E43-modified composite. The improvement in the thermal stability, except for the E43-modified system, may have resulted from the interaction between the organic and inorganic phases. Individual layers of exfoliated clay platelets acted as insulators, and the formation of a tortuous path between the layers also inhibited the passage of volatile degradation products and hence enhanced the thermal stability of the clay composites.

CONCLUSIONS

During the melt compounding of the PP-*g*-MA compatibilizers and organoclay, the intercalation capability of PP-*g*-MA was well known because of the polarity in the MA moiety. In addition to the polarity, the molecular weight, which determined the shear viscosity of PP-*g*-MA, also played a vital role in the effective breakup of clay agglomerates, especially when the organoclay was capable of compensating for the entropy loss of confined polymer chains by improving the chemical affinity with PP-*g*-MA. Regardless of the various types of compatibilizers, all PP-*g*-MA samples had similar degrees of dispersion over a weight ratio

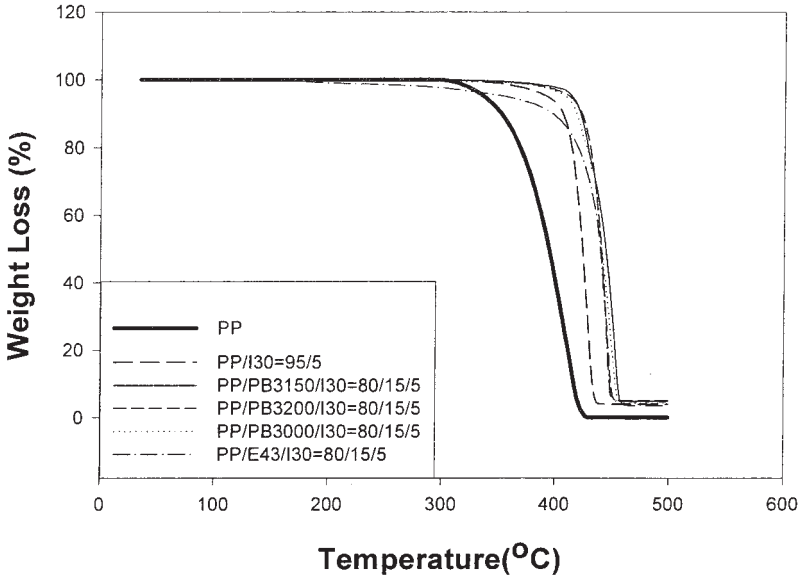

Figure 13 TGA thermograms of the weight loss versus the temperature for PP-*g*-MA-modified PP/I30 nanocomposites.

of 3/1, with the exception of E43. The low molecular weight of E43, which led to a high MI and high-temperature instability, was responsible for the ineffective dispersion of I30 in the E43 matrix. As a result, the relationship between the chemistry of the compatibilizers and the processing conditions had to be coupled because both could affect the exfoliation behavior. Therefore, PP-*g*-MAs with a lower molecular weight and a higher MI needed to be compounded at a lower mixing temperature to generate a high shear viscosity and maintain a reasonable level of torque in the plasticorder, as evidenced by the results for the PB3000/I30 nanocomposites.

Upon the addition of PP-*g*-MA for the modification of the PP/clay mixtures, a series of composite materials based on various combinations of PP, PP-*g*-MA, and organoclay were melt-compounded in a twin-screw extruder. The composites were analyzed to determine the major factors affecting the final morphology and mechanical properties of the composites. There were two important factors that helped the exfoliation and homogeneous dispersion of the clay layers: (1) the intercalation capability of the compatibilizers in the clay layers and (2) the composition of the compatibilizer in the PP/clay composites. Almost complete hybrids were obtained in which PP-*g*-MA showed the proper intercalation capability with a PP-*g*-MA/clay weight ratio greater than 3/1. Rheological characterization by complex viscosity also demonstrated that PP-*g*-MA with a low molecular weight and a high MA content led to better interactions with the clay. However, the addition of lower molecular weight PP-*g*-MA led to less improvement in the mechanical and thermal properties of the PP/PP-*g*-MA/clay nanocomposites.

The authors are grateful to the Instrument Center at National Chung Hsing University for its help with the transmission electron microscopy images.

References

1. Brandmaier, H. E. In Handbook of Reinforcements for Plastics; Milewski, J. V.; Katz, H. S., Eds.; Van Nostrand Reinhold: New York, 1987; Chapter 2, p 6.
2. Gibson, A. G. In Polypropylene: Structure, Blends and Composites; Karger-Kocsis, J., Ed.; Chapman & Hall: London, 1995; Vol. 3, Chapter 2, p 71.
3. Kojima, Y.; Usuki, A.; Kawasumi, M.; Okada, A.; Kurauchi, T.; Kamigaito, J. J Polym Sci Part A: Polym Chem 1993, 31, 983.
4. Giannelis, E. P. Adv Mater 1996, 8, 29.
5. Pinnavaia, T. J.; Lan, T.; Wang, Z.; Shi, H.; Kaviratna, P. D. In Nanotechnology; Chow, G. M.; Gonsalves, K. E., Eds.; ACS Symposium Series 622; American Chemical Society: Washington, DC, 1996; p 251.
6. Zilg, C.; Reichert, P.; Dietsche, F.; Engelhardt, T.; Mülhaupt, R. Kunststoffe 1998, 88, 1812.
7. Alexandre, M.; Dubois, P. Mater Sci Eng 2000, 28, 1.
8. Polymer Clay Nanocomposites; Pinnavaia, T. J.; Beall, G. W., Eds.; Wiley: New York, 2000.
9. Vaia, R. A.; Ishii, H.; Giannelis, E. P. Chem Mater 1993, 5, 1694.
10. Vaia, R. A.; Jandt, K. D.; Kramer, E. J.; Giannelis, E. P. Macromolecules 1995, 28, 8080.
11. Vaia, R. A.; Jandt, K. D.; Kramer, E. J.; Giannelis, E. P. Chem Mater 1996, 8, 2628.
12. Vaia, R. A.; Giannelis, E. P. Macromolecules 1997, 30, 8000–8009.
13. Vaia, R. A.; Vasudevan, S.; Krawiec, W.; Scanlon, L. G.; Giannelis, E. P. Adv Mater 1995, 7, 154.
14. Liu, L.; Qi, Z.; Zhu, X. J Appl Polym Sci 1999, 71, 1133.
15. Cho, J. W.; Paul, D. R. Polymer 2001, 42, 1083.
16. Dennis, H. R.; Hunter, D. L.; Chang, D.; Kim, S.; White, J. L.; Cho, J. W.; Paul, D. R. Polymer 2001, 42, 9513.
17. Kurokawa, Y.; Yasuda, H.; Kashiwagi, M.; Oya, A. J Mater Sci Lett 1997, 16, 1670.
18. Kawasumi, M.; Hasegawa, N.; Kato, M.; Usuki, A.; Okada, A. Macromolecules 1997, 30, 6333.
19. Kato, M.; Usuki, A.; Okada, A. J Appl Polym Sci 1997, 66, 1781.
20. Hasegawa, N.; Kawasumi, M.; Kato, M.; Usuki, A.; Okada, A. J Appl Polym Sci 1998, 67, 87.
21. Oya, A.; Kurokawa, Y.; Yasuda, H. J Mater Sci 2000, 35, 1045.
22. Reichert, P.; Nitz, H.; Klinke, S.; Brandsch, R.; Thomann, R.; Mülhaupt, R. Macromol Mater Eng 2000, 275, 8.
23. Ishida, H.; Campbell, S.; Blackwell, J. Chem Mater 2000, 12, 1260.
24. Wang, H.; Zeng, C.; Svoboda, P.; Lee, L. J. Annu Tech Conf Proc 2001, 59, 2203.
25. Kim, K.-N.; Kim, H.-S.; Lee, J.-W. Annu Tech Conf Proc 2000, 58, 3782.
26. Galgali, G.; Ramesh, G.; Lele, A. Macromolecules 2001, 34, 852.
27. Krishnamoorti, R.; Giannelis, E. Macromolecules 1997, 30, 4097.
28. Solomon, M. J.; Almusallam, A. S.; Seefeldt, K. F.; Somwangthanaroj, A.; Varadan, P. Macromolecules 2001, 34, 1864.
29. Ren, J.; Silva, A. S.; Krishnamoorti, R. Macromolecules 2000, 33, 3379.